

Journal of Materials Chemistry A

Accepted Manuscript



This is an *Accepted Manuscript*, which has been through the Royal Society of Chemistry peer review process and has been accepted for publication.

Accepted Manuscripts are published online shortly after acceptance, before technical editing, formatting and proof reading. Using this free service, authors can make their results available to the community, in citable form, before we publish the edited article. We will replace this *Accepted Manuscript* with the edited and formatted *Advance Article* as soon as it is available.

You can find more information about *Accepted Manuscripts* in the [Information for Authors](#).

Please note that technical editing may introduce minor changes to the text and/or graphics, which may alter content. The journal's standard [Terms & Conditions](#) and the [Ethical guidelines](#) still apply. In no event shall the Royal Society of Chemistry be held responsible for any errors or omissions in this *Accepted Manuscript* or any consequences arising from the use of any information it contains.

Hydrophobic Conjugated Microporous Polymer as a Novel Adsorbent for Removal of Volatile Organic Compounds

Junhui Wang^a, Gang Wang^a, Wanqiu Wang^b, Zhongshen Zhang^a, Zhaotie Liu^b and Zhengping Hao^{*a}

^aDepartment of Environmental Nano-materials,
Research Center for Eco-Environmental Sciences,
Chinese Academy of Sciences, Beijing 100085, China
E-mail: zpinghao@rcees.ac.cn
Fax/Tel: +86-10-62923564

^bKey Laboratory of Applied Surface and Colloid Chemistry,
School of Chemistry & Chemical Engineering,
Shaanxi Normal University, Xi'an 710062, China

Abstract

Conjugated microporous polymers (CMP) synthesized through homocoupling polymerization reaction were investigated as adsorbent for the removal of volatile organic compounds from gas streams. The nitrogen adsorption and desorption data revealed that the resultant CMPs possess micro/mesoporous structure. The results of the static water vapor adsorption experiment indicated that CMP-50 had a more hydrophobic surface than the commercial activated carbon (AC). The adsorption and desorption performance of benzene on CMP-50 under static and dynamic conditions were investigated, comparing with AC. It was found that CMP-50 had high adsorption capacity under wet condition (RH=80%) and fast adsorption kinetics. Moreover, the presence of water vapor in the gas stream had little effect on the adsorption capacity. Taken together, it is expected that this kind materials (such as CMP-50) would be a promising adsorbent for the removal of VOCs vapor from the humid gas streams.

Keywords

Conjugated microporous polymers; Activated carbon; VOCs; Water vapor; Adsorption; Hydrophobicity

1. Introduction

Volatile organic compounds (VOCs) are one of the most important pollutants emitted from anthropical activities such as industrial processes^{1,2}. Most of them not only directly do harm to human health, like causing deformity, pathogenic and even fatal diseases³, but also contribute to serious environmental problems such as formation of particles, destruction of the ozone layer, photochemical smog and global warming, which have a huge potential threat to human beings. Hence the emission of VOCs has triggered increasing awareness focused on the development of control materials and treatment technologies.

Activated carbon (AC) adsorption is applied widely for the removal of VOCs from process effluent stream and pollutants in air^{4,5}. Water vapor would exist at a high concentration in gas streams and moisture is one of the crucial parameters to dictate the efficiency and effectiveness of the adsorption process. It is generally believed that water vapor could compete with the VOCs in the emission stream for adsorption sites on commercial ACs⁶⁻⁹, resulting great decrease in the breakthrough time for the carbon bed and is therefore detrimental to the performance of the carbon filter bed. It is well-known that the damage of VOCs adsorption capacity on ACs in the humid gas streams is attributed to presence of the hydrophilic functional groups,

like hydroxyl, carboxyl and aldehyde — the oxygen-containing functional groups, which are introduced inevitably through the carbonization of ACs¹⁰. Therefore, in order to restrict and avoid such a negative effect, studies have been conducted to develop the methods to lower the hydrophilic surface functional groups of commercial ACs^{11, 12}. However, exploration of a new adsorbent with hydrophobic nature is also a particularly effective way to achieve this goal¹³.

In recent years, organic microporous polymers, like polymers of intrinsic microporosity and hyper-cross-linked polymers have attracted increasing attention in the gas adsorption application because of several advantages^{13, 14}. First, it is possible to control over functionality of organic polymers by a great diversity of synthetic strategies. Second, most organic polymers are highly stable to air, atmospheric moisture and even much more rigorous conditions¹⁵. What is the most important, they can be composed solely of light elements (C, H, O, N, etc. or part of them), which makes it possible to synthesize a certain material without O element. Conjugated microporous polymers (CMPs), one sort of organic microporous polymers, have received considerable research interest because of their fine tuned microporosity, large surface areas and good stability¹⁶⁻²¹, which make them ideal adsorbents for gas adsorption^{16, 17, 19, 21}. However, no studies involving their adsorption behaviors for VOCs and adsorption selectivity from water vapor have been reported to date.

In this research, we successfully synthesized a series of conjugated microporous polymers via using Pd(II)/Cu(I)-catalyzed homocoupling polymerization²² as illustrated in Fig. 1. During the synthesis process, various monomer concentrations

were used and the effects of them on the pore structure were discussed. In order to investigate the adsorption property of the synthesized CMPs, a resultant typical polymer, CMP-50, was selected as a representative adsorbent. Hydrophobic characterization of CMP-50 was evaluated by static adsorption of water vapor and Henry's law constant calculated from the virial equation. Static adsorption and desorption performance as well as the corresponding kinetics of VOCs on CMP-50 were intensively studied. Finally, breakthrough curves of VOCs in the relative humidity of 0% and 80%, respectively, were obtained to evaluate the effect of moisture on the adsorption capacities of CMP-50. Here, benzene, one of the most common and high toxic in VOCs is chosen as the representative adsorbate.

2. Experimental Section

2.1 Preparation of conjugated microporous polymers

The conjugated microporous polymers were synthesized via using Pd(II)/Cu(I) - catalyzed homocoupling polymerization according to the procedure described in the literature²². Typically, 1,3,5-triethynylbenzene (600 mg, 4.0 mmol), bis-(triphenylphosphine)palladium(II) dichloride (85 mg, 4.5mmol%), and copper iodide (22 mg, 4.5mmol%) were dissolved in the mixture of toluene (4 mL) and Et₃N (4.0 mL). The initial monomer concentration was 500 mmol/L. The mixture was then stirred at 70°C under argon atmosphere. After 36 h's reaction, the resulting homocoupled polymer was filtered and washed with chloroform, acetone, water and methanol for several times, and to remove any unreacted monomer or catalyst

residues. Then the polymer was further purified by Soxhlet extraction (methanol) for 3 days. The resulting product was dried at 70°C for 24 h to a constant weight. The resulting polymers were denoted as CMP-x, where x refers to the monomer concentration.

2.2 Characterizations and measurements

The porous properties of CMP-x were investigated by nitrogen adsorption and desorption at liquid nitrogen temperature (77K) using an ASAP2020 volumetric adsorption analyzer (Micromeritics Instrument Corporation). The Brunauer-Emmett-Teller (BET) method was used to calculate the specific surface area. The total pore volume was estimated from the amount adsorbed at a relative pressure of about 0.99. The pore size distribution curves were calculated by analyzing the adsorption branch of the N₂ sorption isotherm using the DFT method. The micropore surface area and micropore volume were calculated by a *t*-plot method. Fourier Transform Infrared (FT-IR) spectra were measured on a Bruker Tensor 27 spectrometer in the range of 600 - 4000 cm⁻¹. The thermogravimetric analysis (TGA) of adsorbents was performed on a TG/DTA analyzer (Setaram, Labsys). The heating rate was 10°C min⁻¹ from 30 to 900°C under a nitrogen flow of 60 mL min⁻¹.

2.3 Static adsorption studies

Adsorption characteristics of benzene and water adsorbate on CMP-x and AC in this study were investigated using an Intelligent Gravimetric Analyzer (IGA), supplied by Hiden Isochema Ltd., Warrington, U.K. The system is an ultrahigh

vacuum (UHV) system comprising a fully computer controlled microbalance, pressure admit and temperature regulation system. The mass was recorded using a microbalance, and the temperature and pressure were computer –controlled. The microbalance has a long-term stability of $\pm 1 \mu\text{g}$ with a weighing resolution of $0.2 \mu\text{g}$. The adsorbent sample ($60 \pm 1 \text{ mg}$) was outgassed to a constant weight, at $< 10^{-6} \text{ Pa}$, at 373K . The liquid used to generate the vapor was degassed fully by repeated evacuation and vapor generation equilibration cycles. The pressure set point accuracy was achieved to 0.02% of the range employed. The set pressure value was maintained by computer control during the course of the experiment. The sample temperature was recorded using a thermocouple located 5 mm from the sample. The equilibrium uptake value was determined as being 90% of the predicted value, calculated in real time using the mass uptake profile. Saturated vapor pressures were calculated using the following equation:

$$\log p_0 = A - \frac{B}{T} + C \log T + DT + ET^2 \quad (1)$$

where p_0 is the saturated vapor pressure (mbar), T is the temperature ($^{\circ}\text{C}$), and A , B , C , D and E are adsorbate dependent constants. The parameters used for each adsorptive are as follows: benzene (A) 31.7718 , (B) -2725.4 , (C) -8.4443 , (D) -5.3535×10^{-9} , (E) 2.7187×10^{-6} ; water (A) 8.09553 , (B) 1747.32 , (C) 235.074 , (D) 0 , (E) 0 .

2.4 Dynamic adsorption measurements

Dynamic adsorption measurements were carried out on a fixed-bed column. The corresponding experimental set-up and method were described in our previous work²³.

Before starting each experiment, the flow rate of the carrier gas and the temperature of the saturator were adjusted so that the required outlet concentration of benzene vapor was reached and kept stable. Then, about 60 mg of sample was packed into the fixed-bed column with an inner diameter of 6 mm and the temperature was maintained at 298K. The samples were degassed at 80°C overnight to remove the physically adsorbed water molecules and other impurities. The concentration of benzene was adjusted to 600 ppm and the total flow rate was 50 mL min⁻¹. In order to investigate the effect of water vapor on the adsorption behavior, 600 ppm of benzene under a relative humidity (RH) of 80% was passed through the adsorption bed. The benzene concentration was recorded on a gas chromatograph (GC) equipped with a flame ionization detector and breakthrough curves were collected. The adsorbed amounts were calculated by the following equation:

$$Q = \frac{F_A t_q}{W} \quad (2)$$

The time t_q is estimated according to Eq. (3):

$$t_q = \int (1 - \frac{C_o}{C_i}) dt - t_D \quad (3)$$

where Q is the adsorbed amount (mmol g⁻¹); F_A is the volumetric flow rate of the carrier gas (mL min⁻¹); W is the net weight of adsorbent (g⁻¹); C_i represents the benzene concentration at the inlet (g mL⁻¹), while C_o is the benzene concentration at the outlet (g mL⁻¹) and t_D is the dead time of the system (min).

3. Results and discussion

3.1 Characterization of CMP-x

Fig. S1 shows the nitrogen adsorption-desorption isotherms of CMP-x and the corresponding pore size distributions obtained by the DFT method. Commercial activated carbon (AC, which was purchased from Beijing Chemical Reagents Company) was studied for comparison. As shown in Fig. S1A, isotherms (a) to (c) belong to Type I according to the IUPAC classification, and the existence of the typical hysteresis loops indicates the mesopore structures in CMP-x²⁴. In contrast, isotherm (d) shows a non-typical hysteresis loop caused by the irregular mesopores of activated carbon. As shown in Fig. S1B, all the polymers exhibit a major peak centered at 1.5 nm, and the amount of the pores around 1.5 nm increase from (a) to (c). However, AC has much more ultra-micropores (<1nm) than the polymers. From Table 1, we can observe that as the monomer concentration decreases, the BET surface area increases, which attributes to the relatively more microvolume (0.17 cm³ g⁻¹ of CMP-50 and 0.10 cm³ g⁻¹ of CMP-500). The nitrogen adsorption and desorption results provide evidence for the existence of both micropores and mesopores in CMP-x.

The FT-IR spectra of CMP-x are shown in Fig. 2. In general, the characteristic absorbance peaks of CMP-x are in accordance with each other, suggesting the persistence of skeleton structure. The absorbance peaks at 1583 cm⁻¹ and 1445 cm⁻¹ are identified as the -C=C- vibration of the aromatic ring²⁵. The peak at 884 cm⁻¹ is attributed to the C-H out-of-plane bending vibration. The peak at 3302 cm⁻¹ and 2197 cm⁻¹ are attributed to the alkyne C-H stretching vibration²⁶ and -C≡C- stretching

vibration²⁷, respectively. From CMP-50 to CMP-500, the intensity of the alkyne C-H stretching vibration increases gradually, suggesting the decreased cross-linking degree, which is consistent with the decreased BET surface area (see Table 1). The evidences in the IR results prove that CMP-x are formed by the homocoupling reaction and their skeletons solely consist of C and H. The FT-IR spectrum of AC is shown in Figure S3. The band at about 3280 cm⁻¹ is attributed to the existence of surface hydroxylic groups and chemisorbed water and the band at 1509 cm⁻¹ can be attributed to the stretching vibration of C=O in conjugated systems such as diketone, ketoester and keto-enol structures²⁸. In addition, the band at 962 cm⁻¹ is assigned to the O-H bending vibration²⁹. The spectrum indicates the presence of the oxygen-containing functional groups in the surface of AC.

The thermal stability of CMP-x and AC were observed by TGA-DTA analysis, as shown in Fig.3. The weight loss at temperature lower than 150 °C is attributed to the loss of adsorbed water and the evaporation of residual organic compounds. The thermal decomposition temperature for CMP-50 is greater than 400°C, which is much higher than that of AC (about 200°C). This result reveals that CMP-50 adsorbent exhibits good thermal stability.

3.2 Static adsorption and desorption behaviors

The conjugated microporous polymer CMP-50 with the biggest BET surface area and open mesostructure was adopted here as a representative sample to estimate its adsorption and desorption properties for VOCs comparing with AC. Fig. 4 shows the

adsorption and desorption isotherms of benzene on CMP-50 (a) and AC (b) at temperatures of 25, 35 and 45°C, respectively. The amount adsorbed decreases with increase of temperature, which is consistent with a physisorption mechanism. The shapes of adsorption and desorption isotherms of benzene for both samples are similar to the nitrogen isotherms, which implies that benzene and nitrogen follow the same adsorption mechanism. It is found that at the very low relative pressure, the amount of benzene on AC has a rapid increase in comparison with CMP, which agrees with augmentation in microporosities of the two adsorbents. The adsorption in micropores at low pressure is a direct consequence of the overlap in the adsorption field from adjacent walls of micropores¹⁴. In comparison with AC (Fig. 4b), the adsorption isotherms of benzene for CMP-50 exhibit capillary condensation steps which is attributed to the presence of mesopores. Therefore, the adsorption isotherms of benzene on CMP-50 exhibit a combination of microporous and mesoporous adsorptive behavior. As shown in Table 2, the equilibrium adsorption capacity of benzene for CMP-50 (6.61 mmol g⁻¹) is higher than that for AC (3.34 mmol g⁻¹) at 35°C. This result can be explained by the fact that the static VOC adsorption capacity is proportional to the total pore volume, in accordance with the literature³⁰.

Water vapor adsorption experiments were conducted to obtain direct information about the surface hydrophobicity of adsorbents occurred. Figure 5 shows the water adsorption isotherms on CMP-50 and AC at 35°C. It is well known that water molecules are adsorbed primarily on the oxygen-containing groups at low relative pressures, followed with the formation of water cluster and then a continuous

adsorption film on the surface, eventually leading to pore filling at high pressure¹⁰. The water vapor uptake at low pressure (p/p_0 is below 0.3) is dependent on the concentration of existing surface hydrophilic sites and at high pressure is related to the pore structure of the adsorbents^{31,32}. In other words, at low pressure, the more hydrophobic surface the adsorbent has, the lower amount of water vapor it adsorbs. It can apparently be observed from Figure 5 that CMP-50 keeps a much lower adsorption amount for water vapor at the whole pressure range. This result clearly indicates that CMP-50 has a much more hydrophobic surface compared with AC, which is mainly attributed to its solely C, H - containing skeleton presented in the IR spectra.

The Henry's law constants, which reflect the affinity between the adsorbent surfaces and the adsorbed gas molecules, can be obtained from the virial equation³³:

$$\ln(n/p) = A_0 + A_1n + A_2n^2 + \dots \quad (4)$$

where n is the amount adsorbed at pressure p , and the first virial coefficient A_0 is related to the Henry's law constant, K_H , by the equation $K_H = \exp(A_0)$. In this study, analysis of the data showed that the higher terms (A_2 , etc.) in the virial equation can be ignored under conditions of low surface coverage³⁴.

Fig. S2 shows the virial graphs for benzene on the CMP-50 at 25, 35 and 45°C. The $\ln(n/p)$ values at low surface coverage ($< \sim 0.2$ wt%) and low pressure ($< \sim 2$ kPa) were subject to higher experimental errors and were not included in the virial graphs. The Henry constants calculated from parameter A_0 of benzene and water on CMP-50 and AC at 35°C are listed in Table 2. As for benzene, the Henry constants increase in

the order of $AC > CMP-50$, which can be explained by strong adsorption energy in micropores³⁵. In the micropores, due to dispersion interactions, field superposition from the close separated opposite pore walls enhances the physical adsorption behavior. However, as far as water, the Henry constant of water on CMP-50 is much smaller than that on AC. This finding supports the above-mentioned conclusion that CMP-50 is more hydrophobic than AC.

3.3 Adsorption and desorption kinetics

In the case of adsorption/desorption, increase/decrease in pressure results in a change in the equilibrium position and mass relaxation occurs to a new equilibrium position. The mass relaxation curve was used to calculate the adsorption/desorption kinetic parameters.

The linear driving force (LDF) model for adsorption is described by the equation³⁶:

$$\frac{M_t}{M_e} = 1 - e^{-kt} \quad (5)$$

where M_t is the uptake at time t , M_e is the equilibrium uptake and k is the rate constant.

The corresponding LDF model for desorption is described by the equation:

$$\frac{M_t}{M_e} = e^{-kt} - 1 \quad (6)$$

where M_e is the amount desorbed at equilibrium and M_t is the amount desorbed at time t ($M_t=0$ at the start, $M_e = -M_t$ and $M_t/M_e = -1$ at equilibrium, after completion of the desorption step).

Fig. 6 and Fig. 7 show typical graphs of M_t/M_e versus time for adsorption and desorption of benzene and water on CMP-50 and AC, respectively, and the corresponding profiles calculated using the LDF model. All the graphs show that the adsorption kinetics obey the LDF model with residuals in the ± 0.04 range. This suggests that the diffusion through the barrier at the pore entrance is the rate-determining step during the adsorption process³⁷. The decrease in effective pore width leads to the development of barriers to surface diffusion into the porous structure.

A comparison of the variation of adsorption and desorption kinetic rate constants of benzene with relative pressure at 35°C on CMP-50 and AC is shown in Fig. 8. The adsorption kinetic rates for CMP-50 (Fig.8a) are basically the same at the overall relative pressure, and higher than those for AC. This observation can be attributed to the fact that the presence of open mesoporous structure in CMP-50 allows high accessibility of the adsorbate. As for the desorption of benzene from CMP-50, the slowest point is in the relative pressure $p/p_0=0.266$, which corresponds with the steepest part of the desorption isotherm (see Fig. 4). At this pressure, it is the most difficult for benzene to desorb from the surface of the adsorbed phase meniscus in the mesopores.

Fig. 8c and d show the variation of adsorption and desorption kinetic rate constants with relative pressure for water on CMP-50 and AC at 35°C. It can be observed that the rate constants for adsorption and desorption follow the same tendency - decrease with increasing relative pressure. At low pressure, water with small molecular

dimensions $(291.7 \times 322.6 \times 388.8 \text{ pm})^{36}$ can easily diffuse into the pores of the adsorbents. As the vapor pressure rises, the surface coverage increases, leading to mono- and multilayer formation in the larger pores. This reduces the effective pore width, and develops barriers to surface diffusion into the porous structure which gives rise to the decrease of the rate constants. However, from Fig. 8d, we can find that in the desorption kinetics there is a slowest point in the relative pressure $p/p_0=0.49$ and from then on the rate constants increase with the rising pressure, which is a typical phenomenon of water desorbed from AC¹⁰. This is due to the pore filling at high pressure, which can be observed from the water vapor adsorption curve in Figure 5. As we expected, this phenomenon does not occur on the CMP-50 adsorbent, which indicates its superhydrophobic surface of inhibiting the development of water cluster, and then the pore filling.

3.4 Dynamic adsorption and desorption behaviors

The investigations of dynamic adsorption and desorption were conducted for the removal of typical VOCs, such as benzene, by representative samples of CMP-50 and AC. A breakthrough measurement is a direct method designed to explore the dynamic performance of VOC adsorption at low concentration³⁰. Figure 9 shows the adsorption breakthrough curves of benzene on CMP-50 and AC at different relative humidity, respectively. To quantitatively elucidate the effect of relative humidity to the adsorption, the breakthrough curves were fitting using the Yoon and Nelson model (Y-N model), expressed as the following equation³⁸:

$$\frac{C_o}{C_i} = \frac{1}{1 + \exp[k'(\tau_0 - t)]} \quad (7)$$

where C_o and C_i are the outlet and inlet concentration of the stream through the fixed bed column (mg L^{-1}), τ_o is the time required for 50% adsorbate breakthrough (min), and κ' is a rate constant that depends on the diffusion characteristics of the mass transfer zone (min^{-1}). It is a simple model and can simulate the breakthrough curves well, as already used for modeling adsorption of chlorinated volatile organic compounds in the fixed bed of hydrophobic hypercrosslinked polymer¹³ and modeling adsorption of benzene and methyl ethyl ketone vapors on activated carbon³⁹ and so forth.

It is shown clearly from the Figure 9 that the breakthrough curves of benzene on CMP-50 and AC under dry conditions and under wet conditions (80% RH) are well fitted by the Y-N model. For the sake of comparison, the calculated adsorption capacities and breakthrough times and rate constants based on the Y-N equation are presented in Table 3. The breakthrough time is calculated as the time at which the outlet concentration is 5% of the inlet concentration. From Table 3, we can see the existence of high concentration water vapor in the gaseous mixture does not induce significant reduction in the adsorption capacity of benzene on CMP-50 — the adsorption efficiency ($Q_{\text{wet}}/Q_{\text{dry}}$) is 88%. On the contrary, the adsorption capacity of AC under wet condition is just 52% of that under dry condition. This result proves the hydrophobic surface property of the CMP-50 adsorbent once again.

In general, the longer the breakthrough time is, the higher the dynamic adsorption capacity becomes. What's more, a more rapid increase in the curve after the breakthrough means less resistance in intraparticle mass transfer³⁹. It can be learned

from Table 3 that under wet condition the breakthrough time of benzene on CMP-50 increases by 384% than that of AC and the rate constant of benzene on CMP-50 increases by 538%, implying less diffusion resistance in the CMP-50 during the adsorption process. This is mainly attributed to its micro/mesoporous property in the region of micropores (0.5-2 nm) and mesopores (2-10 nm). The relative large micropore volume of CMP-50 ensures a high dynamic capacity for benzene, and the mesopores of CMP-50 act as transport pores for benzene molecules diffusing into the internal surface and micro porosity, therefore improve the adsorption kinetics. The dynamic adsorption results indicate CMP-50 possesses the better hydrophobic surface property and less mass transfer resistance than AC. Hence, it is expected that CMP-50 would be a promising adsorbent for the removal of VOCs from high relative humidity streams.

Conclusion

A series of conjugated microporous polymers (CMP) with micro/mesoporous structure were successfully synthesized and investigated on their adsorption property for benzene, a typical organic volatile compound. The static water vapor adsorption amount and Henry' law constant calculated from virial equation proved that CMP-50 was much more hydrophobic than AC. The adsorption kinetic rate constant data revealed that CMP-50 had fast adsorption kinetics for benzene and could not form pore filling of water at high pressure because of its hydrophobic surface. In addition, Yoon and Nelson model could predict the whole breakthrough curve of benzene adsorption on CMP-50 and AC under dry and wet condition. The adsorbed amount of

benzene on CMP-50 under the relative humidity of 80% was about 88% of the corresponding value under dry conditions. What is more, CMP-50 had a good shape of the adsorption breakthrough curves, exhibiting a long breakthrough time and a rapid increase after the breakthrough under wet condition, compared with AC. In general, hydrophobic surface, fast adsorption kinetics, low mass transfer resistance, and the high stability up to 400°C imply this kind of materials (such as CMP-50) would be a promising VOC adsorbent and applied in VOCs control under humid conditions.

Acknowledgement

This work was financially supported by the National Natural Science Foundation (21337003), the National High Technology Research and Development Program of China (No. 2012AA063101), the Strategic Priority Research Program of the Chinese Academy of Sciences (No. XDB05050200), Science Promotion Program of Research Center for Eco-environmental Sciences, CAS (YSW2013B05) and Special Environmental Protection Foundation for Public Welfare Project (201309073).

References

1. Amari, A.; Chlendi, M.; Gannouni, A.; Bellagi, A., Experimental and Theoretical Studies of VOC Adsorption on Acid-Activated Bentonite in a Fixed-Bed Adsorber. *Industrial & Engineering Chemistry Research* **2010**, *49*, (22), 11587-11593.
2. Manjare, S. D.; Ghoshal, A. K., Studies on adsorption of ethyl acetate vapor on

activated carbon. *Industrial & Engineering Chemistry Research* **2006**, *45*, (19), 6563-6569.

3. Ramos, M. E.; Bonelli, P. R.; Cukierman, A. L.; Carrott, M. M. L. R.; Carrott, P. J. M., Adsorption of volatile organic compounds onto activated carbon cloths derived from a novel regenerated cellulosic precursor. *Journal of Hazardous Materials* **2010**, *177*, (1-3), 175-182.

4. Stenzel, M. H., Remove Organics by Activated Carbon Adsorption. *Chemical Engineering Progress* **1993**, *89*, (4), 36-43.

5. Khan, F. I.; Kr Ghoshal, A., Removal of volatile organic compounds from polluted air. *Journal of Loss Prevention in the Process Industries* **2000**, *13*, (6), 527-545.

6. Qi, N.; Appel, W. S.; LeVan, M. D.; Finn, J. E., Adsorption dynamics of organic compounds and water vapor in activated carbon beds. *Industrial & Engineering Chemistry Research* **2006**, *45*, (7), 2303-2314.

7. Cosnier, F.; Celzard, A.; Furdin, G.; B égin, D.; Mar çh é J., Influence of water on the dynamic adsorption of chlorinated VOCs on active carbon: relative humidity of the gas phase versus pre-adsorbed water. *Adsorption Science & Technology* **2006**, *24*, (3), 215-228.

8. Marban, G.; Fuertes, A. B., Co-adsorption of n-butane/water vapour mixtures on activated carbon fibre-based monoliths. *Carbon* **2004**, *42*, (1), 71-81.

9. Kaplan, D.; Nir, I.; Shmueli, L., Effects of high relative humidity on the dynamic adsorption of dimethyl methylphosphonate (DMMP) on activated carbon. *Carbon*

2006, 44, (15), 3247-3254.

10. Foley, N.; Thomas, K.; Forshaw, P.; Stanton, D.; Norman, P., Kinetics of water vapor adsorption on activated carbon. *Langmuir* **1997**, 13, (7), 2083-2089.

11. Menéndez, J. A.; Xia, B.; Phillips, J.; Radovic, L. R., On the modification and characterization of chemical surface properties of activated carbon: microcalorimetric, electrochemical, and thermal desorption probes. *Langmuir* **1997**, 13, (13), 3414-3421.

12. Cosnier, F.; Celzard, A.; Furdin, G.; Begin, D.; Mareche, J. F.; Barres, O., Hydrophobisation of active carbon surface and effect on the adsorption of water. *Carbon* **2005**, 43, (12), 2554-2563.

13. Long, C.; Liu, P.; Li, Y.; Li, A. M.; Zhang, Q. X., Characterization of Hydrophobic Hypercrosslinked Polymer as an Adsorbent for Removal of Chlorinated Volatile Organic Compounds. *Environmental Science & Technology* **2011**, 45, (10), 4506-4512.

14. Dou, B.; Li, J.; Wang, Y.; Wang, H.; Ma, C.; Hao, Z., Adsorption and desorption performance of benzene over hierarchically structured carbon-silica aerogel composites. *Journal of Hazardous Materials* **2011**, 196, 194-200.

15. Jiang, J.-X.; Su, F.; Trewin, A.; Wood, C. D.; Niu, H.; Jones, J. T.; Khimyak, Y. Z.; Cooper, A. I., Synthetic control of the pore dimension and surface area in conjugated microporous polymer and copolymer networks. *Journal of the American Chemical Society* **2008**, 130, (24), 7710-7720.

16. Thomas, A., Functional materials: from hard to soft porous frameworks. *Angewandte Chemie International Edition* **2010**, 49, (45), 8328-8344.

17. Weber, J.; Thomas, A., Toward stable interfaces in conjugated polymers: microporous poly (p-phenylene) and poly (phenyleneethynylene) based on a spirobifluorene building block. *Journal of the American Chemical Society* **2008**, *130*, (20), 6334-6335.
18. Weber, J.; Antonietti, M.; Thomas, A., Microporous networks of high-performance polymers: Elastic deformations and gas sorption properties. *Macromolecules* **2008**, *41*, (8), 2880-2885.
19. Jiang, J. X.; Su, F.; Trewin, A.; Wood, C. D.; Campbell, N. L.; Niu, H.; Dickinson, C.; Ganin, A. Y.; Rosseinsky, M. J.; Khimyak, Y. Z., Conjugated microporous poly (aryleneethynylene) networks. *Angewandte Chemie International Edition* **2007**, *46*, (45), 8574-8578.
20. Jiang, J. X.; Su, F.; Niu, H.; Wood, C. D.; Campbell, N. L.; Khimyak, Y. Z.; Cooper, A. I., Conjugated microporous poly(phenylene butadiynylene)s. *Chemical Communications* **2008**, (4), 486-8.
21. Li, A.; Lu, R. F.; Wang, Y.; Wang, X.; Han, K. L.; Deng, W. Q., Lithium-doped conjugated microporous polymers for reversible hydrogen storage. *Angewandte Chemie International Edition* **2010**, *49*, (19), 3330-3.
22. Li, A.; Sun, H.-X.; Tan, D.-Z.; Fan, W.-J.; Wen, S.-H.; Qing, X.-J.; Li, G.-X.; Li, S.-Y.; Deng, W.-Q., Superhydrophobic conjugated microporous polymers for separation and adsorption. *Energy & Environmental Science* **2011**, *4*, (6), 2062.
23. Hu, Q.; Li, J. J.; Hao, Z. P.; Li, L. D.; Qiao, S. Z., Dynamic adsorption of volatile organic compounds on organofunctionalized SBA-15 materials. *Chemical*

Engineering Journal **2009**, *149*, (1-3), 281-288.

24. Pierotti, R.; Rouquerol, J., Reporting physisorption data for gas/solid systems with special reference to the determination of surface area and porosity. *Pure and Applied Chemistry* **1985**, *57*, (4), 603-619.

25. Li, C.; Liu, J.; Shi, X.; Yang, J.; Yang, Q., Periodic mesoporous organosilicas with 1, 4-diethylenebenzene in the mesoporous wall: synthesis, characterization, and bioadsorption properties. *The Journal of Physical Chemistry C* **2007**, *111*, (29), 10948-10954.

26. Kariuki, B. M.; Harris, K. D. M.; Philp, D.; Robinson, J. M. A., A triphenylphosphine oxide-water aggregate facilitates an exceptionally short C-H center dot center dot center dot O hydrogen bond. *Journal of the American Chemical Society* **1997**, *119*, (51), 12679-12680.

27. Yan, Z.; Ren, H.; Ma, H.; Yuan, R.; Yuan, Y.; Zou, X.; Sun, F.; Zhu, G., Construction and sorption properties of pyrene-based porous aromatic frameworks. *Microporous and Mesoporous Materials* **2013**, *173*, 92-98.

28. P.Cambier, Infrared study of goethites of varying crystallinity and particle size: I. Interpretation of OH and lattice vibration frequencies. *Clay Minerals* **1986**, *21*, 191-200.

29. S. Biniak; G. S.; J. Siedlewski; A. Swiatkowski, The characterization of activated carbons with oxygen and nitrogen surface groups. *Carbon* **1997**, *35*, (12), 1799-1810.

30. Kosuge, K.; Kubo, S.; Kikukawa, N.; Takemori, M., Effect of pore structure in mesoporous silicas on VOC dynamic adsorption/desorption performance. *Langmuir*

2007, 23, (6), 3095-3102.

31. Karanfil, T.; Dastgheib, S. A., Trichloroethylene adsorption by fibrous and granular activated carbons: aqueous phase, gas phase, and water vapor adsorption studies. *Environmental Science & Technology* **2004**, 38, (22), 5834-5841.

32. Mowla, D.; Do, D.; Kaneko, K., Adsorption of water vapor on activated carbon: a brief overview. *Chemistry and Physics of Carbon* **2003**, 28, 229-229.

33. Bell, J. G.; Zhao, X.; Uygur, Y.; Thomas, K. M., Adsorption of Chloroaromatic Models for Dioxins on Porous Carbons: The Influence of Adsorbate Structure and Surface Functional Groups on Surface Interactions and Adsorption Kinetics. *The Journal of Physical Chemistry C* **2011**, 115, (6), 2776-2789.

34. Zhao, X.; Xiao, B.; Fletcher, A.; Thomas, K., Hydrogen adsorption on functionalized nanoporous activated carbons. *The Journal of Physical Chemistry B* **2005**, 109, (18), 8880-8888.

35. Dou, B.; Li, J.; Hu, Q.; Ma, C.; He, C.; Li, P.; Hu, Q.; Hao, Z.; Qiao, S., Hydrophobic micro/mesoporous silica spheres assembled from zeolite precursors in acidic media for aromatics adsorption. *Microporous and Mesoporous Materials* **2010**, 133, (1-3), 115-123.

36. Fletcher, A. J.; Yüzak, Y.; Thomas, K. M., Adsorption and desorption kinetics for hydrophilic and hydrophobic vapors on activated carbon. *Carbon* **2006**, 44, (5), 989-1004.

37. Berenguer-Murcia, Á.; Fletcher, A. J.; García-Martínez, J.; Cazorla-Amoros, D.; Linares-Solano, Á.; Thomas, K. M., Probe molecule kinetic studies of adsorption on

MCM-41. *The Journal of Physical Chemistry B* **2003**, *107*, (4), 1012-1020.

38. Yoon, Y. H.; NELSON, J. H., Application of gas adsorption kinetics I. A theoretical model for respirator cartridge service life. *The American Industrial Hygiene Association Journal* **1984**, *45*, (8), 509-516.

39. Long, C.; Li, Y.; Yu, W.; Li, A., Removal of benzene and methyl ethyl ketone vapor: comparison of hypercrosslinked polymeric adsorbent with activated carbon. *Journal of Hazardous Materials* **2012**, *203*, 251-256.

Table 1. Textural properties of CMP-x and AC

Material	BET surface area (m ² g ⁻¹)	Average pore diameter (nm)	Total pore volume (cm ³ g ⁻¹)	Micropore volume (cm ³ g ⁻¹)	Micropore area (cm ³ g ⁻¹)
CMP-50	880	3.1	0.63	0.17	316
CMP-250	828	6.4	1.10	0.14	272
CMP-500	566	5.0	0.64	0.10	177
AC	704	3.1	0.45	0.20	380

Table 2. Equilibrium adsorption capacities Q^e and Henry constants of benzene and water on CMP-50 and AC at 35°C

Sample	Equilibrium adsorption capacities		Henry constants	
	Q^e (mmol g ⁻¹)		K_H ($\times 10^{-7}$ mol g ⁻¹ Pa ⁻¹)	
	Benzene	Water	Benzene	Water
CMP-50	6.61	3.23	78.89	1.36
AC	3.34	20.84	442.79	12.04

Table 3. Dynamic adsorption capacities of CMP-50 and AC and breakthrough characteristics of benzene adsorption calculated from Y-N model

Material	Dynamic adsorption capacity		Q_{wet}/Q_{dry} (%)	Breakthrough time (min) (RH=80%)	Rate constant κ' (min ⁻¹) (RH=80%)	R^2
	Q (mmol g ⁻¹)					
	$Q_{RH=0\%}$	$Q_{RH=80\%}$				
CMP-50	1.23	1.08	88%	43.44	0.51	0.999
AC	1.72	0.90	52%	8.97	0.08	0.993

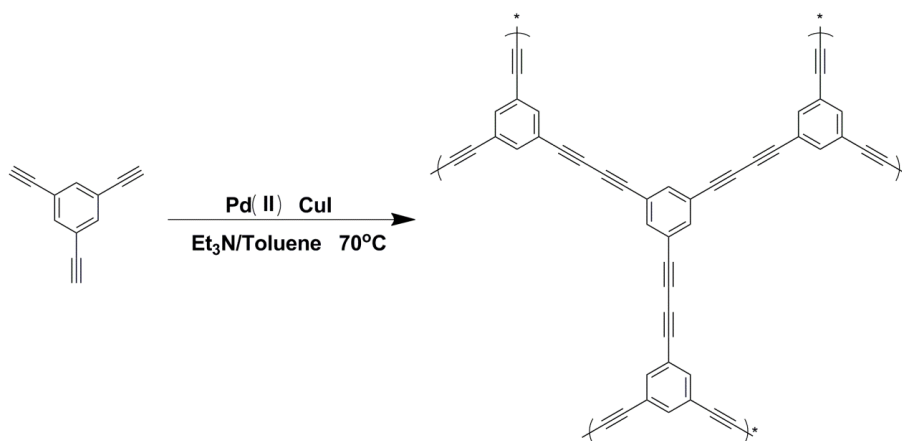


Figure 1. Schematic illustration for the synthesis of CMP-x

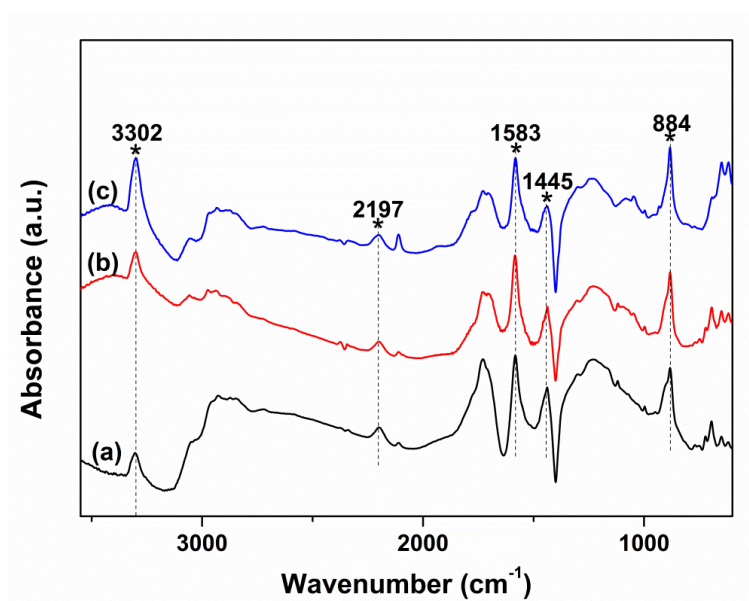


Figure 2. FT-IR spectra of patterns for CMP-50 (a), CMP-250 (b), CMP-500 (c)

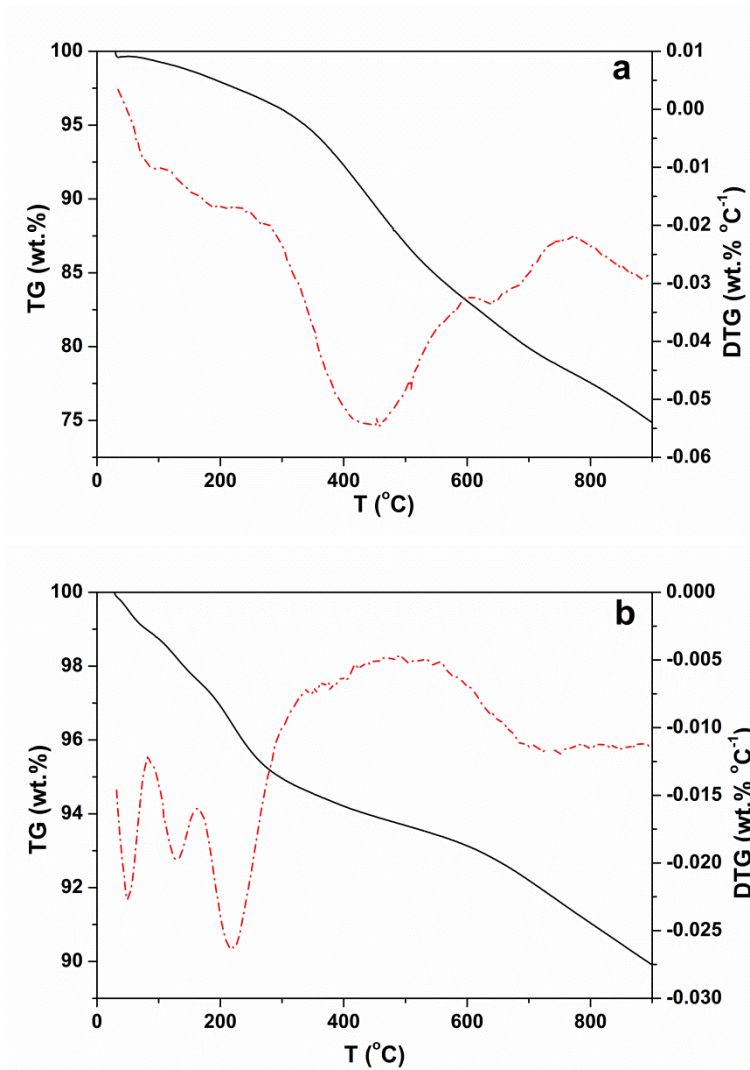
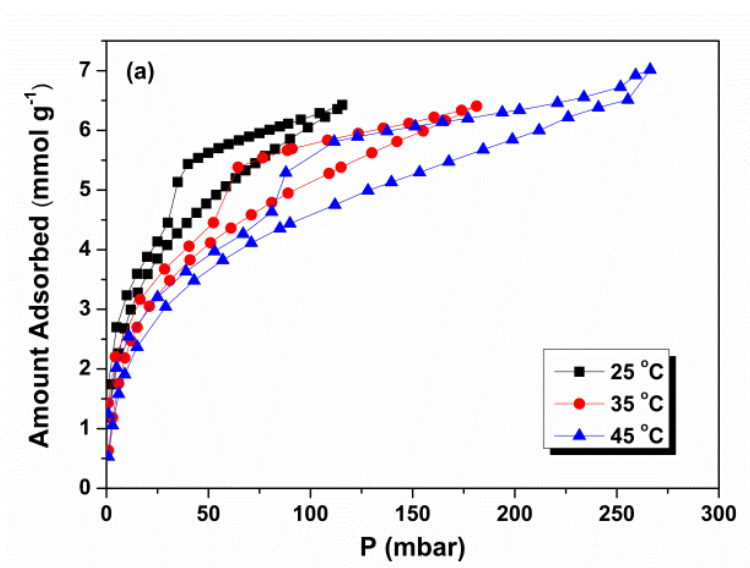


Figure 3. TG and DTG curves for CMP-50 (a) and AC (b) materials



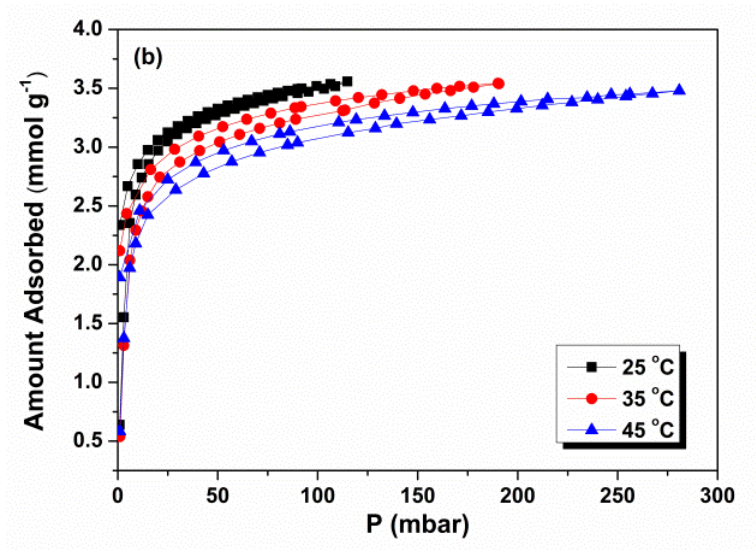


Figure 4. Adsorption and desorption isotherms of benzene on CMP-50 (a) and AC (b) materials at different temperatures

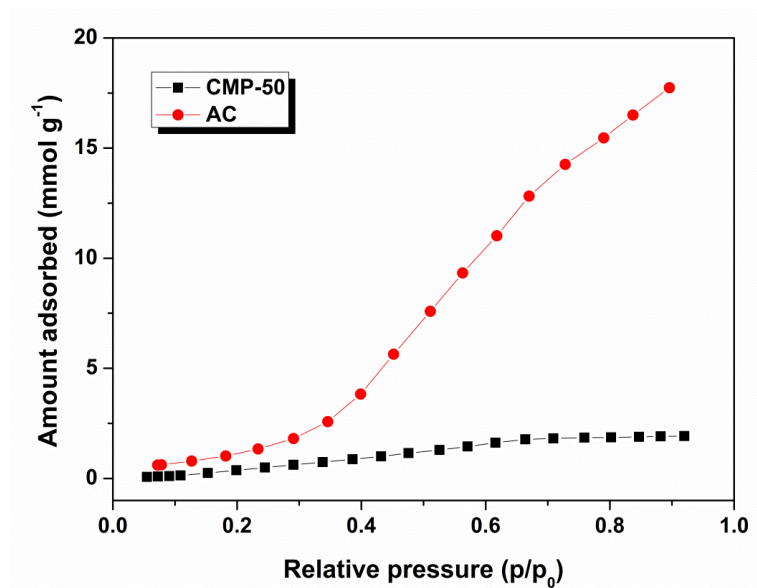


Figure 5. Adsorption isotherms of water vapor on CMP-50 and AC at 35 °C

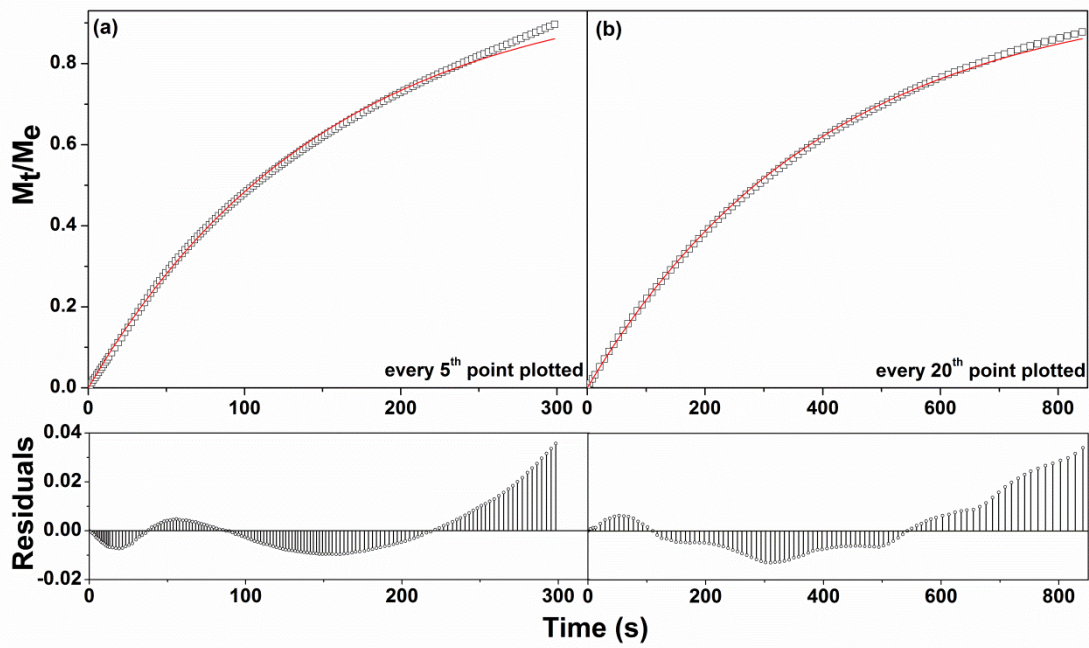


Figure 6. Variation of M_t/M_e versus time for benzene adsorption on CMP-50 and AC at 35°C
 (a) CMP-50: 80.4166-81.0194 mbar ($p/p_0=0.6234-0.6281$); (b) AC: 11.89-12.01 mbar
 ($p/p_0=0.0608-0.0617$)

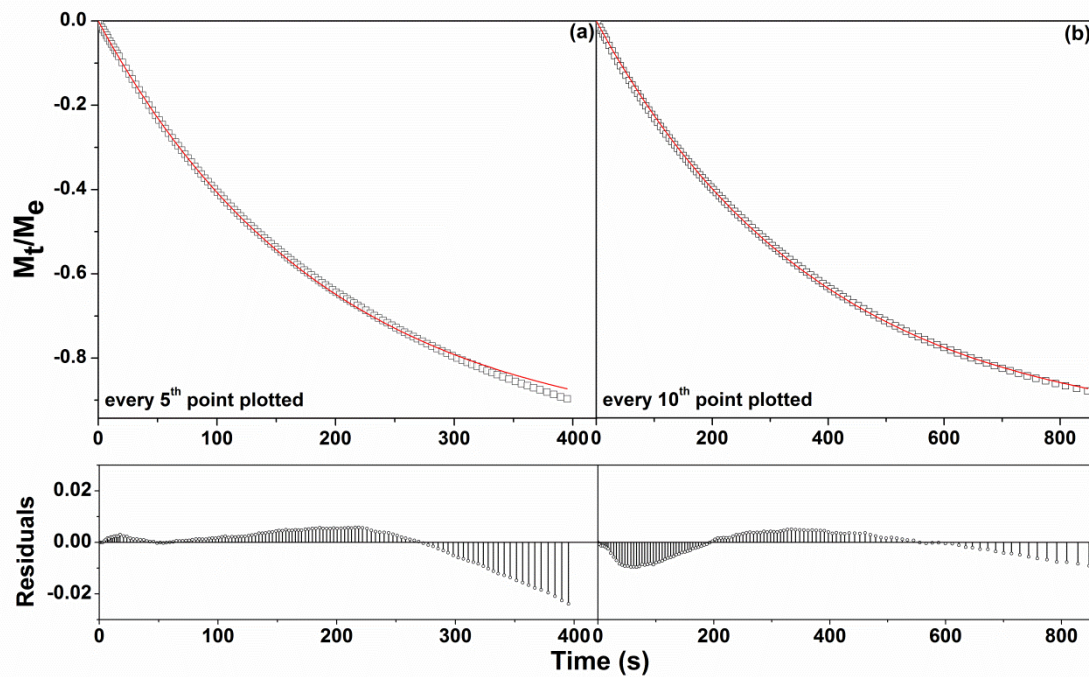


Figure 7. Variation of M_t/M_e versus time for water desorption on CMP-50 and AC at 35°C
 (a) CMP-50: 35.83-35.62 mbar ($p/p_0=0.1834-0.1825$); (b) AC: 45.27-45.06 mbar
 ($p/p_0=0.2317-0.2306$)

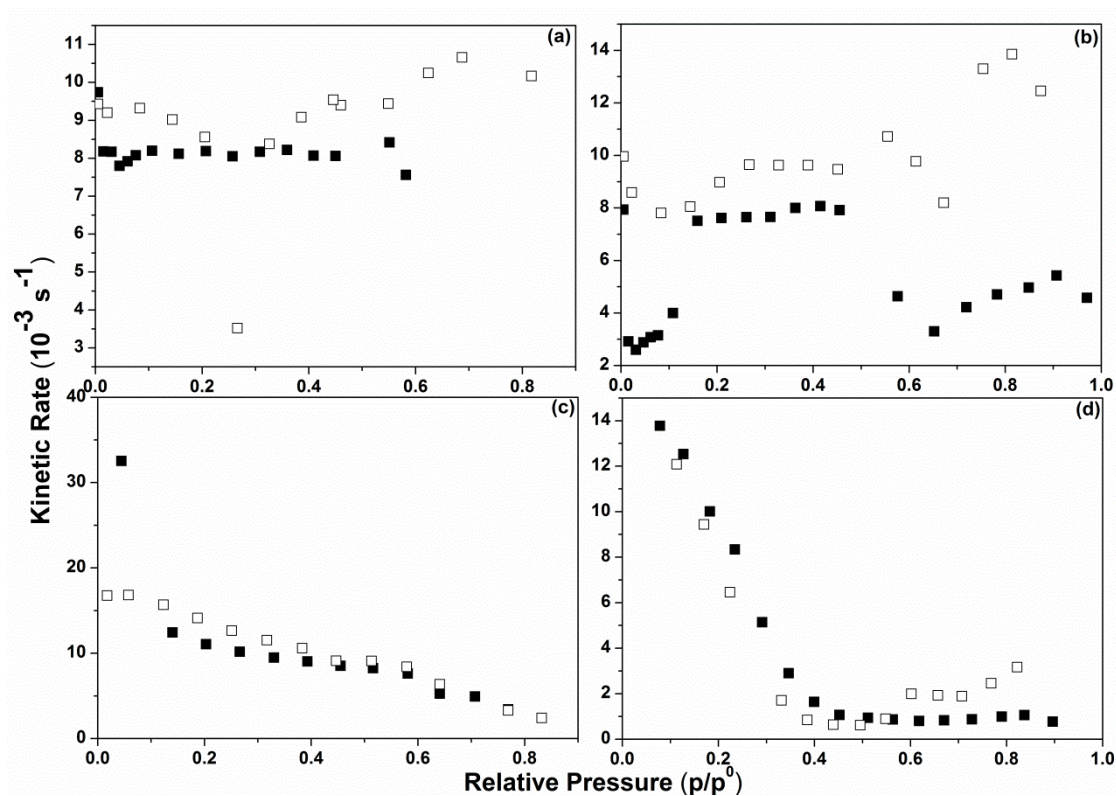
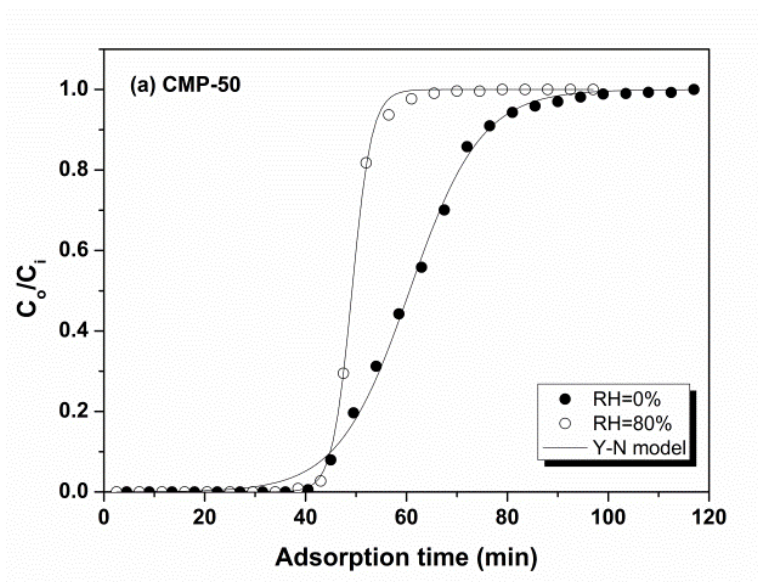


Figure 8. Variation of rate constants for adsorption (filled symbols) and desorption (open symbols) on/from the samples with relative pressure at 35°C.
 (a) benzene on CMP-50; (b) benzene on AC; (c) water on CMP-50; (d) water on AC



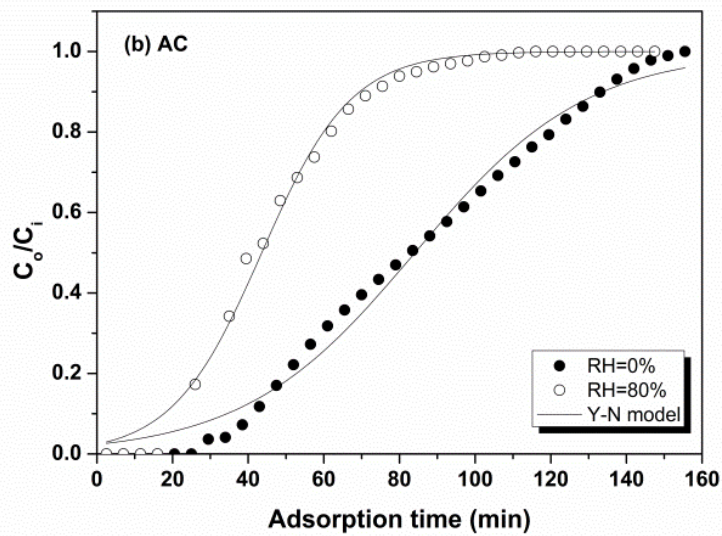
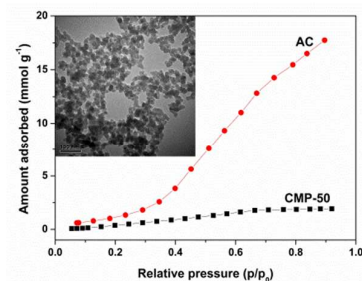


Figure 9. The breakthrough curves for benzene adsorption on CMP-50 (a) and AC (b) materials. Curves with filled symbols represent results obtained under dry conditions and curves with empty symbols represent results obtained under wet conditions (80% RH)



Conjugated microporous polymers with micro/mesoporous structure exhibit hydrophobic nature and represent a promising VOCs adsorbent under humid conditions.